RESEARCH BRIEF

Androgen Receptor Signaling Regulates DNA Repair in Prostate Cancers

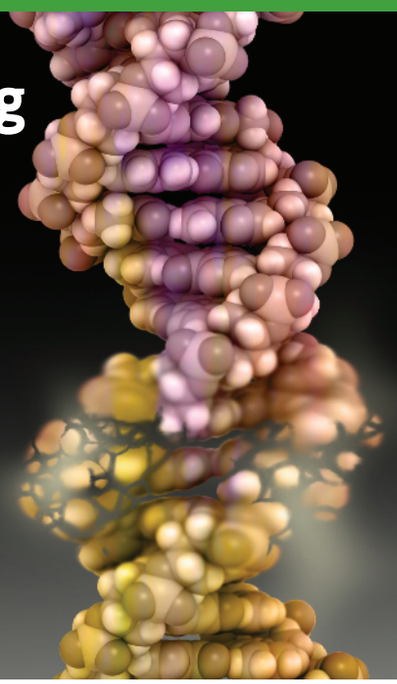

William R. Polkinghorn[1,4], Joel S. Parker[10,11], Man X. Lee[1], Elizabeth M. Kass[2], Daniel E. Spratt[1], Phillip J. Iaquinta[1], Vivek K. Arora[1,5], Wei-Feng Yen[3], Ling Cai[1], Deyou Zheng[9], Brett S. Carver[1,6], Yu Chen[1,5], Philip A. Watson[1], Neel P. Shah[1], Sho Fujisawa[8], Alexander G. Goglia[4], Anuradha Gopalan[7], Haley Hieronymus[1], John Wongvipat[1], Peter T. Scardino[6], Michael J. Zelefsky[1], Maria Jasin[2], Jayanta Chaudhuri[3], Simon N. Powell[4], and Charles L. Sawyers[1]

ABSTRACT We demonstrate that the androgen receptor (AR) regulates a transcriptional program of DNA repair genes that promotes prostate cancer radioresistance, providing a potential mechanism by which androgen deprivation therapy synergizes with ionizing radiation. Using a model of castration-resistant prostate cancer, we show that second-generation antiandrogen therapy results in downregulation of DNA repair genes. Next, we demonstrate that primary prostate cancers display a significant spectrum of AR transcriptional output, which correlates with expression of a set of DNA repair genes. Using RNA-seq and ChIP-seq, we define which of these DNA repair genes are both induced by androgen and represent direct AR targets. We establish that prostate cancer cells treated with ionizing radiation plus androgen demonstrate enhanced DNA repair and decreased DNA damage and furthermore that antiandrogen treatment causes increased DNA damage and decreased clonogenic survival. Finally, we demonstrate that antiandrogen treatment results in decreased classical nonhomologous end-joining.

SIGNIFICANCE: We demonstrate that the AR regulates a network of DNA repair genes, providing a potential mechanism by which androgen deprivation synergizes with radiotherapy for prostate cancer.
Cancer Discov; 3(11); 1245–53. ©2013 AACR.

See related commentary by Bartek et al., p. 1222.

INTRODUCTION

Multiple clinical trials comparing radiotherapy plus androgen deprivation therapy (ADT) versus radiotherapy alone for high-risk, and more recently intermediate-risk, prostate cancer show significant improvement in disease-free and overall survival with the addition of ADT (1, 2). Furthermore, post-treatment biopsy series demonstrate improved local control when ADT is added to radiotherapy (3). In light of these and other studies, combining ADT with radiotherapy for high-risk prostate cancer has been the standard of care for nearly 20 years, yet the mechanism by which ADT improves patient

Authors' Affiliations: [1]Human Oncology Pathogenesis Program, [2]Developmental Biology Program, and [3]Immunology Program; Departments of [4]Radiation Oncology, [5]Medicine, [6]Surgery, and [7]Pathology; [8]Molecular Cytology Core Facility, Memorial Sloan-Kettering Cancer Center; [9]Department of Genetics, Albert Einstein College of Medicine, New York, New York; [10]Department of Genetics; and [11]Lineberger Comprehensive Cancer Center, University of North Carolina, Chapel Hill, North Carolina

Note: Supplementary data for this article are available at Cancer Discovery Online (http://cancerdiscovery.aacrjournals.org/).

Corresponding Author: Charles L. Sawyers, Memorial Sloan-Kettering Cancer Center, 1275 York Avenue, New York, NY 10065. Phone: 646-888-2138; Fax: 646-888-3407; E-mail: sawyersc@mskcc.org

doi: 10.1158/2159-8290.CD-13-0172

outcomes remains unknown. Furthermore, it is unknown whether ADT benefits a subset of patients substantially or all patients with prostate cancer to a smaller degree.

Given the compelling body of clinical evidence, many have sought to elucidate how inhibiting the androgen receptor (AR) potentiates ionizing radiation. Using *in vitro* and *in vivo* models, the addition of ADT to ionizing radiation has been shown to increase prostate cancer cell death (4). A number of mechanisms have been explored to explain the increase in cell death when ADT is combined with ionizing radiation, including decreased tumor cell hypoxia (5), decreased DNA repair (6), or simply decreased AR-mediated cell growth independent of direct synergy (7). Surprising light has recently been shed on additional interrelationships between AR and DNA repair, including a role for AR in mediating prostate cancer–specific translocations following high-dose ionizing radiation (8) and the discovery that the DNA repair protein, PARP1, is an important cofactor for AR transcriptional activity (9).

Defining the mechanism by which ADT increases prostate cancer radioresponse has never been more clinically relevant given the recently demonstrated success of second-generation antiandrogens in the treatment of castration-resistant patients (10, 11). Given the clinical potential of deploying these new agents as part of radiotherapy for primary disease coupled with the ability now to leverage prostate cancer genomics data to help define genetic mechanisms in a less biased way, it is critical to reexamine the basic biologic question of how AR signaling promotes prostate cancer radioresistance.

RESULTS

We began with an unbiased query of how gene expression is perturbed when a clinically validated xenograft model of castration-resistant prostate cancer, LNCaP-AR, is treated with the second-generation antiandrogen ARN-509 (12, 13). After 4 days of treatment with ARN-509, transcriptome analysis was performed by Illumina HT12 expression array. Standard gene set enrichment analysis (GSEA) was performed, and, to our surprise, three out of the top 10 gene sets that were enriched in the control versus ARN-509–treated groups represented DNA repair gene sets; in total, six DNA repair gene sets comprised the top 50 enriched gene sets (Fig. 1A and Supplementary Table S1).

Given the unexpected result of ADT decreasing DNA repair gene expression in the castration-resistant model, we next sought to determine whether there was an association of AR transcriptional output with DNA repair genes in primary, castration-sensitive human prostate tumors (14). This set of primary prostate cancer tumors represents the appropriate group to analyze, as this is the disease state treated with ADT and radiotherapy. First, we determined the variance of canonical AR transcriptional output, using a well-known signature derived by Hieronymus and colleagues (14, 15) across primary human prostate cancer tumors. Again, to our surprise, we observed a large spectrum of canonical AR output (Fig. 1B). Given this variance of AR output across primary prostate cancer tumors, we next asked whether there was a correlation between a composite score of canonical AR output, as previously calculated (16), and a composite score of the enriched DNA repair genes from the previous xenograft experiment. Upon this analysis, we indeed found a significant correlation ($P < 0.001$) between canonical AR output and the enriched DNA repair genes (Fig. 1C). Next, to define the most robust signature of AR-associated DNA repair genes without limiting ourselves to the enriched genes from the initial xenograft experiment, we more broadly asked which of the DNA repair genes in all of the six combined DNA repair gene sets (294 genes) were most associated with canonical AR output in the primary human prostate cancer dataset (Fig. 1D and Supplementary Table S2). Filtering for an association with canonical AR output ($P < 0.01$ and $r > 0$), we defined an "AR-associated DNA repair gene" signature of 144 DNA repair genes that were significantly associated with canonical AR output.

Given the association of canonical AR output with DNA repair gene expression in primary prostate cancers, we next sought to determine using an *in vitro* model which, if any, of these DNA repair genes are transcriptionally regulated by androgen. We selected the most widely studied prostate cancer cell line, LNCaP, to model primary prostate cancer. After treating the LNCaP prostate cancer cell line with synthetic androgen (R1881) for 2 days and comparing with vehicle-treated [dimethyl sulfoxide (DMSO)] cells, we measured gene expression level changes by RNA-seq and identified AR target genes by AR chromatin immunoprecipitation sequencing (ChIP-seq). We first confirmed that our newly defined, 144-gene AR-associated DNA repair gene signature was in fact enriched by GSEA in the androgen-treated samples, in addition to other well-known AR signatures such as Nelson and colleagues (ref. 17; Fig. 2A). Of the 144 genes that comprise the AR-associated DNA repair signature, we next identified those genes whose expression was increased by androgen and that contained AR binding sites (Fig. 2B). Thirty-two genes were both induced by androgen and exhibited AR peaks in their enhancers (32) or promoter (1), suggesting that these represented *bona fide* AR target genes (Fig. 2B and C and Supplementary Fig. S2). Motif analysis of the AR binding peaks of these 32 genes revealed the classic consensus AR binding site (Fig. 2D).

We next sought to determine whether the reduction in DNA repair gene expression observed with androgen deprivation was associated with (i) reduced DNA repair and (ii) increased DNA damage. Using the same *in vitro* LNCaP model, we exposed prostate cancer cells, pretreated for 2 days with either synthetic androgen (1 nmol/L R1881) or mock (DMSO), to 2 Gy of ionizing radiation, and γ-H2AX foci were quantified. Comparing the γ-H2AX foci in the two conditions, we found that in androgen-depleted conditions the foci peaked later and higher and resolved more slowly, consistent with decreased repair (Fig. 3A). Because γ-H2AX foci represent a surrogate, indirect marker of unrepaired breaks, we next sought to measure DNA damage itself. To do so, we used the neutral Comet assay that directly measures DNA double-strand breaks (DSB). The findings of the Comet assay under the same conditions recapitulated the results obtained by analyzing γ-H2AX foci (Fig. 3B). Of note, at baseline after 48 hours of pretreatment (time 0), mock-treated cells demonstrated increased γ-H2AX foci and increased DNA damage by Comet assay. However, after normalizing the findings from both assays to each condition's respective time 0, the post-ionizing radiation findings of relative decreased repair and

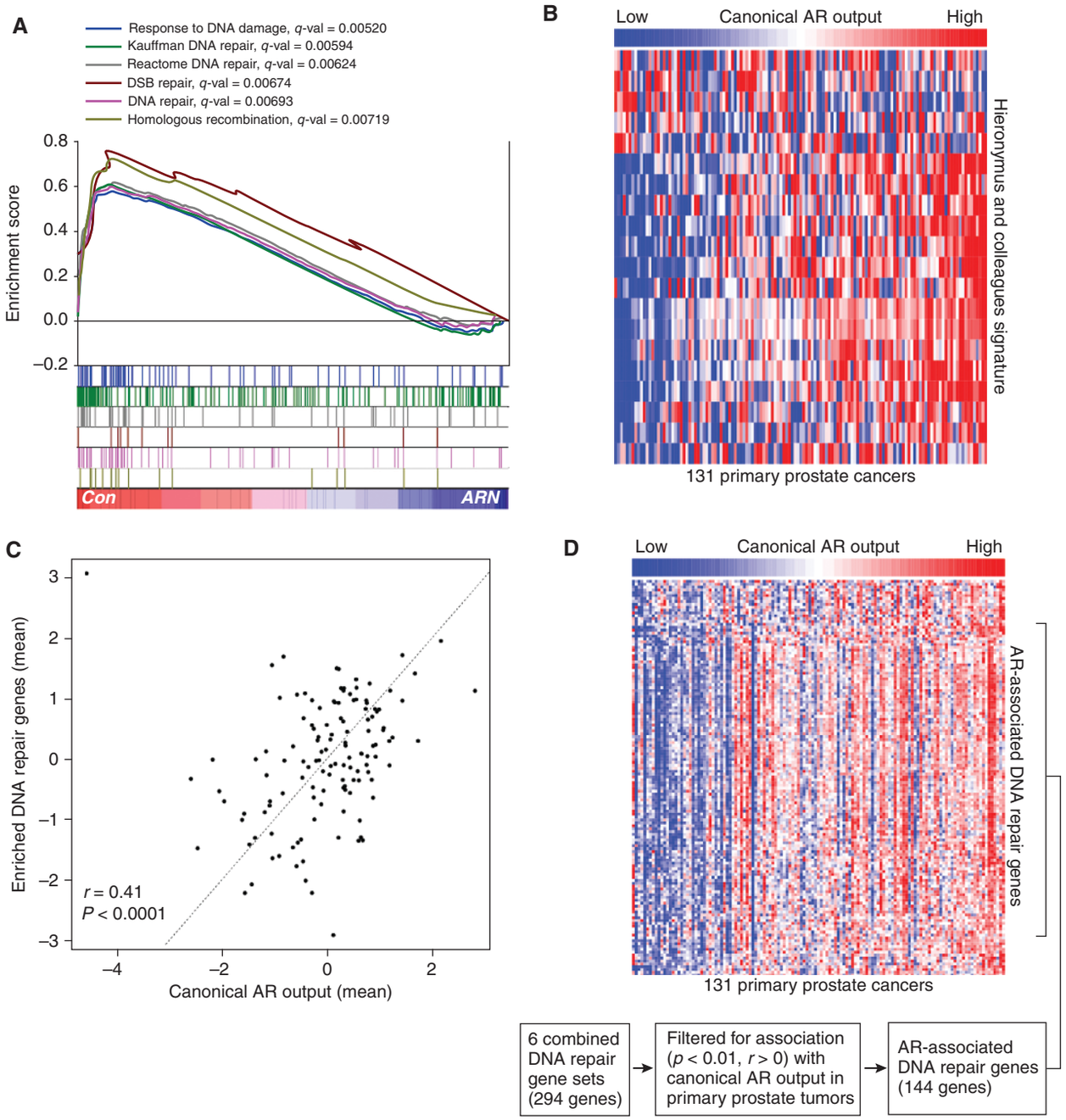

Figure 1. AR transcriptional output is associated with expression of DNA repair genes. **A,** GSEA of second-generation antiandrogen (ARN-509) treatment of a castration-resistant xenograft model (LNCaP-AR). Xenografts were treated with 4 days of either control (red) or ARN-509 (blue). **B,** heatmap demonstrating a wide spectrum of AR transcriptional output ("canonical AR output"), calculated using Hieronymus and colleagues (15), across a cohort of 131 primary prostate cancer tumors. **C,** correlation between enriched DNA repair genes from the xenograft experiment (**A**) and canonical AR output in primary prostate cancer cohort. **D,** union of top six enriched DNA repair gene sets from xenograft experiment filtered for an association with canonical AR output ($P < 0.01$ and $r > 0$) in same human cohort. Primary prostate tumors ranked from low to high canonical AR output, left to right, with corresponding heatmap of associated 144 DNA repair genes ("AR-associated DNA repair" signature).

increased damage persisted (Supplementary Fig. S1). Given the surprising result that even in the absence of ionizing radiation androgen deprivation alone exhibited increased DNA damage as compared with androgen-treated cells, we next asked whether treatment with ARN-509 would also increase DNA damage relative to control. After 48 hours of ARN-509 (1 μmol/L) treatment versus mock (DMSO), we found increased DNA damage in LNCaP cells, a finding we then demonstrated in two additional cell lines, LNCaP-AR and VCaP (Fig. 3C).

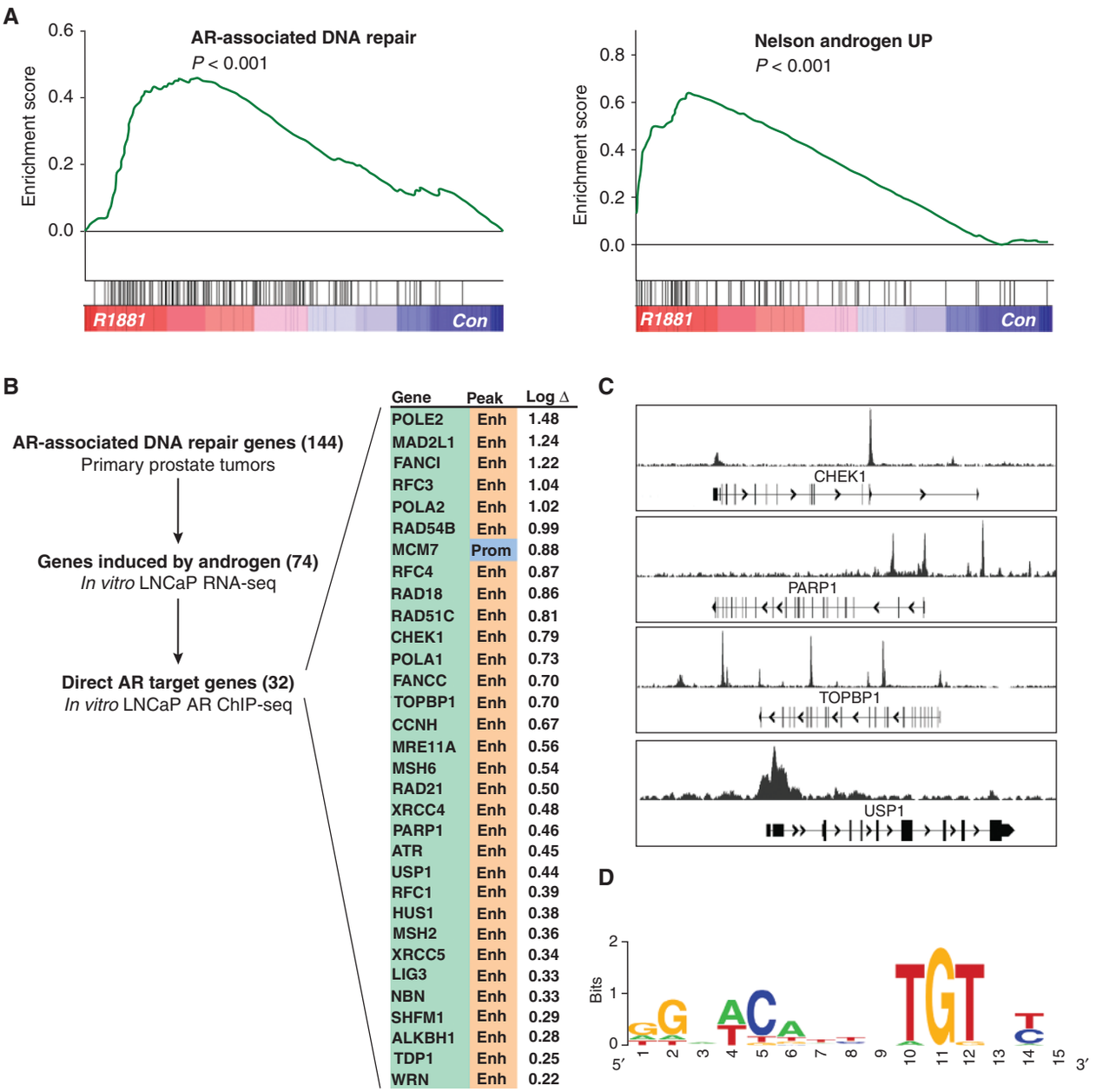

Figure 2. A network of DNA repair genes is both induced by androgen and represents AR target genes. **A,** GSEA of LNCaP cell line grown in charcoal-stripped serum in the presence of exogenous androgen (R1881), red, or control, blue. Previously defined AR-associated DNA repair signature enriched for in addition to other well-established AR signatures, such as Nelson and colleagues (17). **B,** of the 144-gene AR-associated DNA repair signature, 72 genes are significantly induced by R1881, and of these genes 32 represent AR target genes by ChIP-seq. **C,** examples of AR peaks on representative DNA repair genes. **D,** motif analysis of the AR binding peaks of these 32 genes revealed the classic consensus AR binding site.

Given these findings, we next asked whether antiandrogen-treated cells compared with mock-treated cells exhibited decreased cell viability following ionizing radiation. To do so, we used the classic clonogenic assay using the LNCaP cell line and demonstrated that treatment with ARN-509 (1 μmol/L) compared with mock (DMSO) resulted in decreased cell survival (Fig. 3D). To further address the possibility that the enhanced radiosensitivity observed with ADT is not due to partial synchronization of rapidly dividing cells into more radiosensitive phases of the cell cycle, we measured the percentage of LNCaP cells in G_1, S, and G_2–M in androgen-deprived cells (DMSO) compared with a range of doses of R1881 in charcoal-stripped serum, each for 48 hours. The percentage of cells across the phases of the cell cycle did not change, yet increasing concentrations of androgen resulted in increased cell growth except for the highest concentration (10 nmol/L; Supplementary Fig. S2). We repeated this analysis for LNCaP cells treated with ARN-509 versus control for

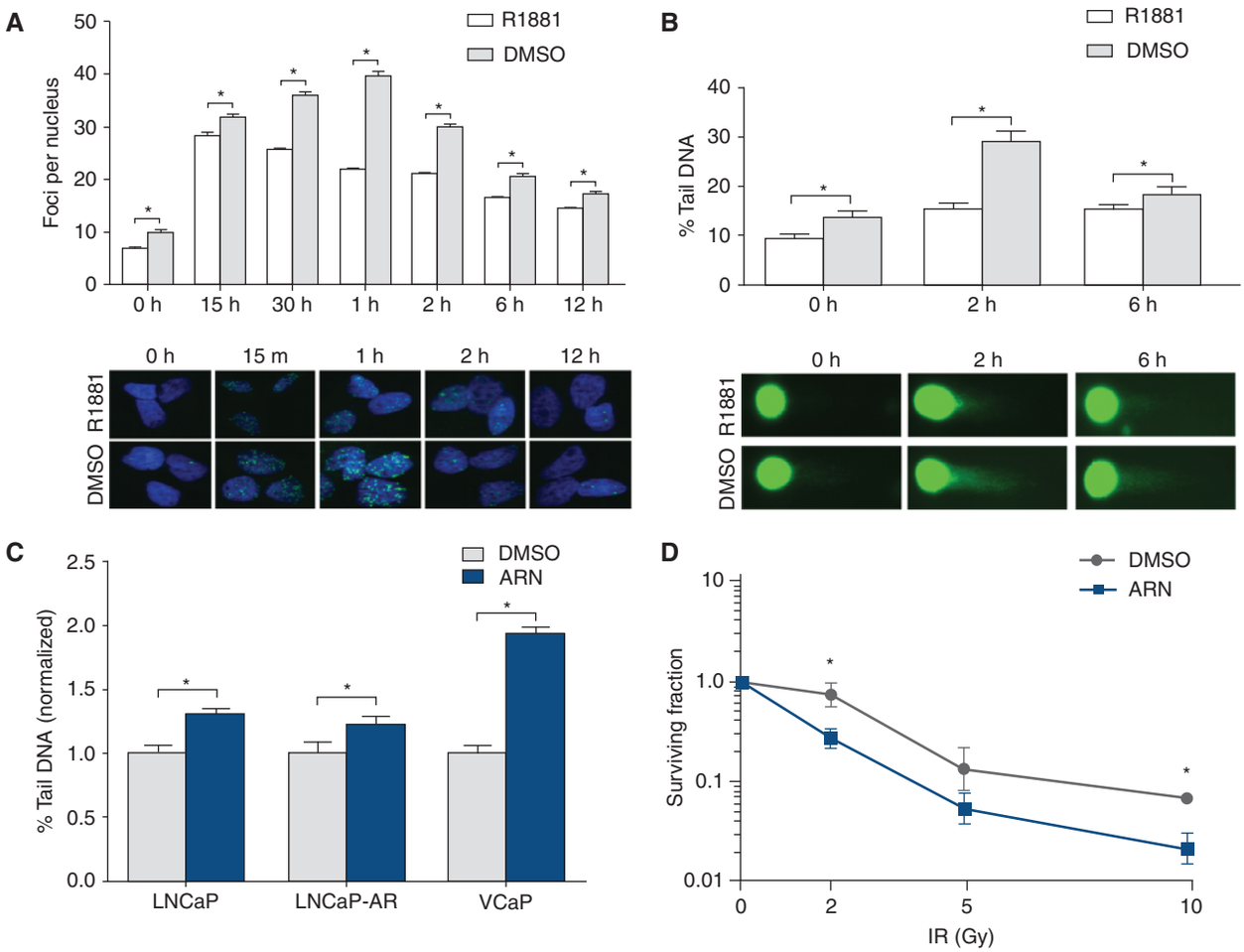

Figure 3. Enhanced DNA repair in prostate cancer cells treated with androgen plus ionizing radiation (IR), decreased DNA repair and survival of cells treated with antiandrogen plus ionizing radiation. **A,** LNCaP cells, pretreated with either synthetic androgen (R1881) or mock, exposed to 2 Gy of ionizing radiation, with DNA damage measured by γ-H2AX foci. Under androgen-depleted conditions, the foci peaked later and higher and resolved more slowly (*, $P < 0.001$). **B,** neutral Comet assay of LNCaP cell line, showing increased DSBs when cells were irradiated under androgen-deprived conditions (*, $P < 0.001$). **C,** neutral Comet assay of LNCaP, LNCaP-AR, and VCaP cells after 48 hours of treatment with second-generation antiandrogen (ARN-509) versus mock demonstrates increased DSBs (*, $P < 0.001$). **D,** clonogenic survival assay of LNCaP cells demonstrates decreased survival when irradiated in the presence of ARN-509 versus mock (*, $P \leq 0.02$).

48 hours, and again found no meaningful change in cell-cycle distribution (Supplementary Fig. S3).

Given these findings that AR transcriptionally regulates a network of DNA repair genes and that antiandrogen treatment increases DNA damage and radiosensitizes cells, we next sought to determine which DNA repair pathways are functionally abrogated by ARN-509 (Fig. 4A). Because the DNA DSBs induced by ionizing radiation are thought to be repaired by classical nonhomologous end-joining (C-NHEJ) and homologous recombination, we focused upon these repair pathways.

To assess the effects of antiandrogen treatment on C-NHEJ, we used the transient V(D)J recombination assay as previously described (Fig. 4B; refs. 18, 19). The V(D)J recombination substrate along with RAG1 and RAG2 expression vectors were transfected into LNCaP cells that had been pretreated for 48 hours with either mock (DMSO) or ARN-509 (1 μmol/L). In this assay, rescued substrate plasmids that fail to undergo C-NHEJ–dependent recombination only express the ampicillin (Amp)-resistant gene, whereas those that successfully undergo recombination express both Amp- and chloramphenicol (Cam)-resistant genes. Therefore, after transforming bacteria with the rescued substrate, a recombination frequency can be calculated by the ratio of colonies grown on the Amp + Cam plates compared with the ampicillin plates. Compared with control treatment, ARN-509–treated cells demonstrated significantly decreased C-NHEJ–mediated recombination (>60%), comparable with that seen with stable LIG4 knockdown (Fig. 4C and Supplementary Fig. S4). Next, to assess the effects of antiandrogen treatment on homologous recombination, we used the transient DR-GFP assay, a widely used repair reporter assay for studying homologous recombination (Fig. 4D; ref. 20). DR-GFP contains direct repeats of two defective *GFP*

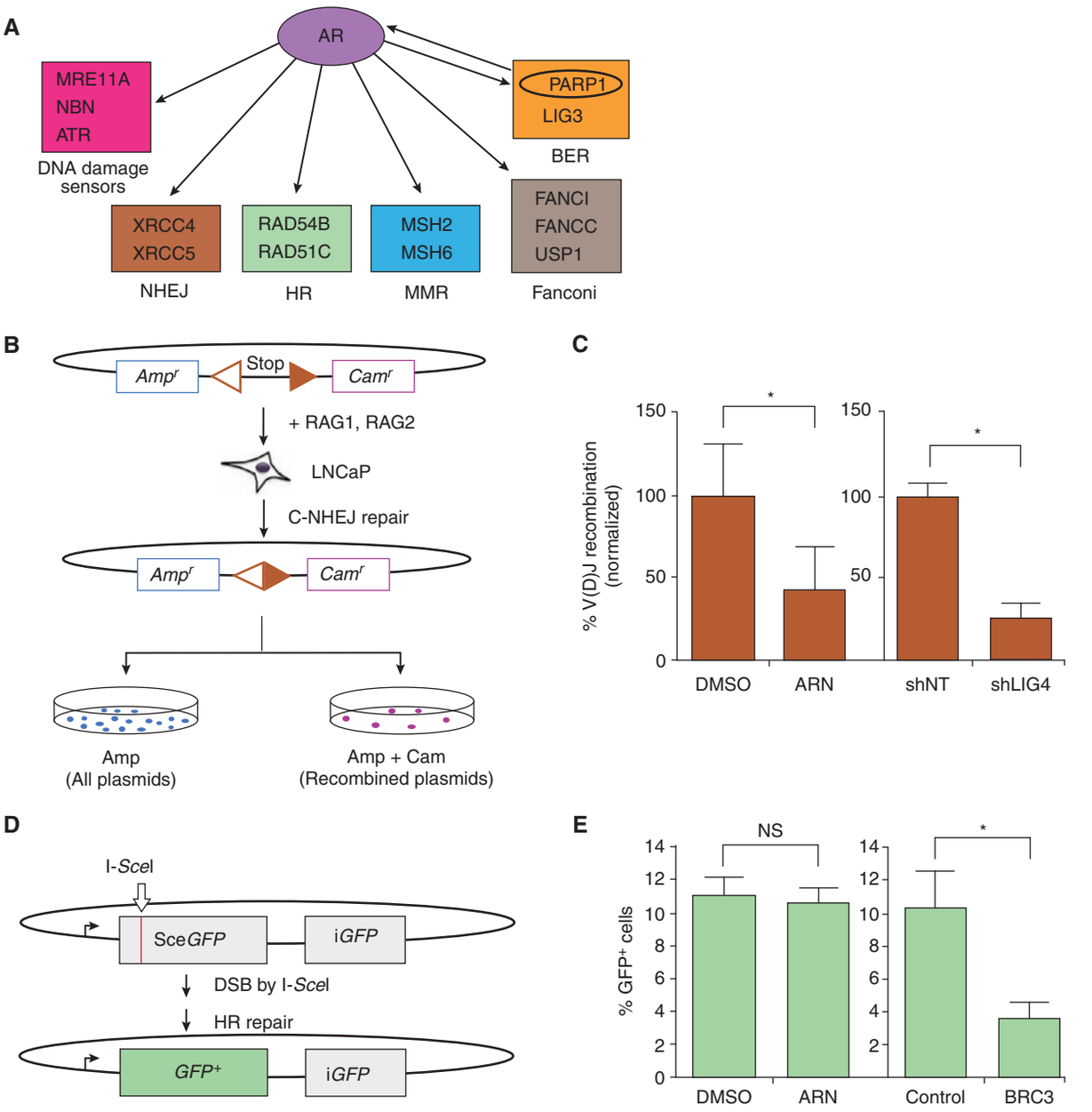

Figure 4. AR regulates a network of DNA repair genes. **A,** the AR-regulated transcriptome includes a number of DNA repair genes, one of which is the known AR cofactor PARP1. Other AR-regulated DNA repair genes play important roles in DNA damage sensing, non-NHEJ, homologous recombination (HR), mismatch repair (MMR), and the Fanconi pathway. **B,** schematic outlining the transient V(D)J recombination assay in which substrate along with RAG1 and RAG2 expression vectors are transfected into cells, after which bacteria are transformed with the rescued substrate and plated. Rescued substrate plasmids that fail to undergo recombination by C-NHEJ only express the ampicillin-resistant gene, whereas those that successfully undergo recombination express both ampicillin- and chloramphenicol-resistant genes. Recombination frequency can be calculated by the ratio of colonies grown on the Amp + Cam plates compared with the ampicillin plates. **C,** compared with control-treated LNCaP cells, treatment with ARN-509 significantly ($P < 0.01$) decreases C-NHEJ as measured using transient V(D)J recombination assay. The magnitude of effect is comparable with that observed when LIG4, a known mediator of C-NHEJ, has been stably knocked down in a LNCaP cell line ($P < 0.01$). **D,** schematic outlining transient DR-GFP assay, in which DR-GFP contains direct repeats of two defective *GFP* genes with the upstream repeat containing a recognition site for the I-*Sce*I endonuclease. When a DSB is introduced by I-*Sce*I followed by successful homologous recombination repair using the downstream copy as a template, it produces a functional *GFP* gene; GFP+ cells are scored by flow cytometry. **E,** compared with control-treated LNCaP cells, treatment with ARN-509 has no measurable effect upon homologous recombination repair as measured by the transient DR-GFP assay ($P = 0.38$; $n = 4$ transfections), whereas expression of the dominant negative BRC3 peptide ($n = 3$) results in an approximately 2.8-fold reduction in homologous recombination compared with vector control ($n = 2$; $P = 0.015$).

genes with the upstream repeat containing a recognition site for the I-*Sce*I endonuclease. A DSB induced by I-*Sce*I followed by gene conversion with the downstream copy results in a functional *GFP* gene, and GFP$^+$ cells can be scored by flow cytometry. Using this assay, no significant difference in homologous recombination was observed between the treated and control cells, in contrast to the 2.8-fold reduction in homologous recombination observed with expression of BRC3, a peptide known to interfere with homologous recombination (Fig. 4E; ref. 21).

DISCUSSION

Androgens, acting through AR, regulate a complex transcriptional program for both prostate cancer growth and differentiation, with recent data demonstrating unique sets of AR target genes in castration-sensitive versus -resistant tumors (22). In this study, we discover a network of DNA repair genes that comprises part of the complex AR-regulated transcriptome. Our data establish that AR signaling increases the expression of DNA repair genes and, in parallel, promotes prostate cancer radioresistance by accelerating repair of ionizing radiation–induced DNA damage. Collectively, these data provide a strong mechanistic rationale for the observed synergy between ADT and radiotherapy.

Clinical trials of ADT plus radiotherapy have been unable to answer the question of whether ADT benefits all patients modestly or a subset to a greater degree. The surprising spectrum of AR output that we observe in primary prostate cancer tumors suggests that ADT may preferentially benefit those patients with high AR transcriptional output and, consequently, high expression of DNA repair genes. Therefore, in a similar manner that patients with breast cancer are selected for antiestrogen therapy by a molecular determinant of response (estrogen receptor/progesterone receptor status), perhaps it is possible to select patients with prostate cancer who will receive ADT along with radiotherapy (as opposed to radiotherapy alone) based on a tumor's AR output. This hypothesis could be tested using pathologic specimens from one of the landmark clinical trials comparing ADT and radiotherapy with radiotherapy alone.

The discovery that AR activity, among its other known biologic effects, also regulates DNA repair could have implications beyond the question of how ADT synergizes with radiotherapy. First, the finding that C-NHEJ can be dynamically modulated via inhibition of a nuclear hormone receptor/transcription factor represents a new kind of mechanism by which to abrogate this important pathway. Second, it remains to be determined whether the other identified AR-regulated DNA repair genes play a functional role in their respective pathways (e.g., mismatch repair, base excision repair, and Fanconi pathway) when their expression levels are modulated by AR (Fig. 4A). Finally, recent genomic studies demonstrate that in comparison with primary tumors, one of the hallmarks of castration-resistant prostate cancer seems to be widespread genomic instability (14, 23). The possibility that the therapeutic intervention of ADT itself during the several-year period of castration sensitivity may contribute to the genomic instability observed in castration-resistant tumors raises a number of important future directions for investigation.

METHODS

LNCaP/AR Xenografts

LNCaP/AR xenografts were established in castrate mice as described previously and, once established, were treated for 4 days with either 10 mg/kg ARN-509 plus vehicle (1% carboxymethyl cellulose, 0.1% Tween-80, and 5% DMSO) or vehicle alone (12). RNA was isolated as per the standard protocol and expression profiling performed using IlluminaHT-12 array (Arora and colleagues; in preparation). GSEA (24) was used to test for pathway level differential expression. Discovery analysis of the xenograft transcriptomes used all gene sets listed in both the curated (c2) and Gene Ontology (c5) of the Broad Institute's Molecular Signature Databases (MSigDB).

Determining Association between Canonical AR Output and DNA Repair Genes

Canonical AR output was quantified using an unweighted summed score of the *n*-gene AR-responsive gene signature defined by Hieronymus and colleagues (15). The initial set of DNA repair candidates was taken as the union of the six DNA repair–associated signatures resulting from the xenograft experiment. The correlation between the AR signature and each candidate gene was calculated. Results were filtered to identify all DNA repair–associated genes with significant (Pearson correlation, $P < 0.01$) positive correlations. The resulting candidates were summarized to the within sample mean as a relative measure of the signature. Spearman correlation was used to test for significant relationship between the AR and DNA repair signatures.

LNCaP RNA-Seq/ChIP-Seq

LNCaP cells were grown in described conditions in triplicate, and RNA was isolated by the RNeasy Mini Kit (Qiagen) with the additional steps of lysate homogenization using QIAshredder (Qiagen) and DNase digestion using the RNase-Free DNase Set (Qiagen). Samples were prepared and libraries were created using TruSeq RNA Sample Preparation Kit v2 (Illumina), which included a poly-A selection step. Libraries were pooled at 2 nm concentration and the samples were then subject to cBot cluster generation using TruSeq Rapid PE Cluster Kit (Illumina). The amplified libraries were sequenced using the TruSeq Rapid SBS Kit on the HiSeq 2500 (Illumina). mRNA-seq data were aligned with Mapsplice (25) and genes were quantified with RNA-Seq by Expectation Maximization (26). Gene expression estimates were log transformed and upper quartile normalized. Differential expression was measured using unequal variance *t* test to identify candidate genes. GSEA analysis of the cell line data was used to test whether the 144 AR-associated DNA repair genes were associated with R1881 treatment relative to DMSO. AR ChIP-Seq was performed according to Cai and colleagues (in preparation).

Cell Irradiation

All described doses of ionizing radiation were delivered using Cs-137 irradiator (Shepherd Mark, Model 68) at a dose rate of 184 cGy/min and at a turntable speed of 6 rpm.

γ-H2AX Assay

LNCaP cells were grown in described conditions for 2 days on CC2-coated, four-chamber slides (Nunc Lab-Tek II; Thermo Scientific), approximately 20,000 cells per well in 500 μL total volume, and following ionizing radiation were washed and fixed with 4% paraformaldehyde and 0.2% Triton X-100. Slides were blocked with 10% FBS and 0.5% Triton X-100, and the primary antibody (γ-H2AX; Millipore) was incubated overnight at 4°C. Slides were then washed, incubated with secondary antibody (Alexa Fluor 488 Dye; Life Technologies) for 1 hour at room temperature, and stained for 4′,6-diamidino-2-phenylindole. Slides were scanned by confocal microscopy (LSM

5 LIVE) with a 20×/0.8NA objective and foci were counted by MetaMorph image analysis software (Molecular Devices). For each time point, on average, foci of 2,000 separate nuclei were counted.

Neutral Comet Assay

LNCaP, LNCaP-AR, and VCaP cells were grown in described conditions for 2 days and neutral Comet assay was performed using CometAssay Electrophoresis System (Trevigen) as per assay protocol (27).

Clonogenic Assay

LNCaP cells were grown in 10-cm tissue culture–treated polystyrene dishes (BD Falcon) in described conditions for 2 days before irradiation. Cells received either 0, 2, 5, or 10 Gy of ionizing radiation, and were subsequently replated in respective conditions into 6-well, tissue culture–treated polystyrene plates (BD Falcon) in a series of 1:3 dilutions (24,000, 8,000, 2,667, 867, 289, and 96 cells/well) at each dose. Lethally irradiated HeLa feeder cells (400,000) were added to each well to promote colony formation. Plates were incubated for 14 days, then washed and fixed with methanol, and stained with 0.2% crystal violet (Sigma) in 10% formalin (Sigma). Plates were scanned by GelCount (Oxford Optronix), and colonies were counted using GelCount software. Clonogenic survival curves were generated as previously described.

Western Blot Analysis

Whole-cell lysates were prepared using 10% M-PER lysis buffer and clarified by centrifugation. Proteins were separated by 4% to 12% SDS-PAGE gel and transferred onto polyvinylidene difluoride (PVDF) membranes (Invitrogen). After primary antibody incubation (LIG4 and GAPDH; Abcam) for 1 hour at room temperature, washings, and incubation with secondary antibodies, blots were developed with a chemiluminescence system (Pierce).

Transient V(D)J Recombination Assay

The transient V(D)J recombination assay was performed as described according to Gauss and Lieber (18, 19). The V(D)J recombination substrate plasmid along with RAG1 and RAG2 expression vectors were transfected into LNCaP cells (2×10^6) pretreated for 48 hours with either mock (DMSO) or ARN-509 (1 μmol/L), or the same cell line infected with shNT (nontargeting) or sh*LIG4* lentiviral vectors (Sigma-Aldrich). Plasmids were retrieved 48 hours following transfection, and electrocompetent bacteria (Mega-X DH10B; Invitrogen) were then transformed with the rescued substrate plasmids and plated on both ampicillin and Amp + Cam plates. Bacteria were plated at 1:1,000–5,000 dilution for ampicillin plates and 1:10–50 dilution for Amp + Cam plates to grow colonies at numbers that could be quantified by manual counting. Substrate plasmids that failed to undergo recombination by C-NHEJ only expressed the ampicillin-resistant gene (Amp^r), whereas plasmids that underwent successful recombination expressed both Amp^r and chloramphenicol-resistant (Cam^r) genes. Recombination efficiency was calculated by the ratio of the colonies grown on the Amp + Cam plates to the ampicillin plates.

DR-GFP Assay

To measure DSB repair by homologous recombination, 2×10^6 LNCaP cells were nucleofected with 0.7 μg of DR-GFP plasmid and 2 μg I-*Sce*I expression vector (pCBASce) and 1.3 μg empty vector (pCAGGS) or 3.3 μg pCAGGS or for a positive control 2 μg NZEGFP and 2 μg pCAGGS (20). After transfection, cells were immediately plated in regular medium containing 1 μmol/L ARN-509 or control (DMSO). For BRC3 experiments, 2×10^6 LNCaP cells were nucleofected with 0.7 μg of DR-GFP plasmid, 2 μg I-SceI expression vector (pCBASce), and 2 μg of BRC3 expression plasmid or empty vector (pCAGGS; ref. 21). Flow cytometry was performed 48 hours after transfection to analyze GFP expression.

Cell Lines

LNCaP and VCaP cell lines used in this article were purchased directly from American Type Culture Collection and cultured according to specifications. LNCaP-AR is an AR-overexpressing (wild-type) cell line originally derived from parental LNCaP; the LNCaP-AR cell line was authenticated for AR overexpression by immunoblot.

Disclosure of Potential Conflicts of Interest

J. Wongvipat has ownership interest (including patents) in a UCLA patent for ARN-509. C.L. Sawyers has ownership interest (including patents) in ARN-509 (co-inventor) and is a consultant/advisory board member of Aragon Phamaceuticals. No potential conflicts of interest were disclosed by the other authors.

Authors' Contributions

Conception and design: W.R. Polkinghorn, P.J. Iaquinta, N.P. Shah, H. Hieronymus, M.J. Zelefsky, M. Jasin, S.N. Powell, C.L. Sawyers

Development of methodology: W.R. Polkinghorn, J.S. Parker, E.M. Kass, D.E. Spratt, D. Zheng, B.S. Carver, Y. Chen, A.G. Goglia, J. Chaudhuri, S.N. Powell

Acquisition of data (provided animals, acquired and managed patients, provided facilities, etc.): W.R. Polkinghorn, E.M. Kass, D.E. Spratt, V.K. Arora, W.-F. Yen, L. Cai, S. Fujisawa, A.G. Goglia, A. Gopalan, J. Wongvipat

Analysis and interpretation of data (e.g., statistical analysis, biostatistics, computational analysis): W.R. Polkinghorn, J.S. Parker, M.X. Lee, D.E. Spratt, P.J. Iaquinta, V.K. Arora, D. Zheng, B.S. Carver, Y. Chen, N.P. Shah, S. Fujisawa, A.G. Goglia, H. Hieronymus, M. Jasin, S.N. Powell, C.L. Sawyers

Writing, review, and/or revision of the manuscript: W.R. Polkinghorn, D.E. Spratt, W.-F. Yen, B.S. Carver, Y. Chen, A. Gopalan, P.T. Scardino, M. Jasin, C.L. Sawyers

Administrative, technical, or material support (i.e., reporting or organizing data, constructing databases): W.R. Polkinghorn, M.X. Lee, D.E. Spratt, P.A. Watson, J. Wongvipat

Study supervision: M.J. Zelefsky, C.L. Sawyers

Acknowledgments

The authors thank M.R. Lieber (University of Southern California, Los Angeles, CA) for graciously providing the plasmids for the transient V(D)J recombination assay. In addition, W.R. Polkinghorn wishes to thank T.G. Bivona for his encouragement and friendship and C.L. Sawyers both for the opportunity to pursue this important question and for teaching him to become a scientist along the way.

Grant Support

This work was supported by the Prostate Cancer Foundation, Creativity Award (2011).

Received April 21, 2013; revised September 5, 2013; accepted September 10, 2013; published OnlineFirst September 11, 2013.

REFERENCES

1. Bolla M, Gonzalez D, Warde P, Dubois JB, Mirimanoff RO, Storme G, et al. Improved survival in patients with locally advanced prostate cancer treated with radiotherapy and goserelin. N Engl J Med 1997;337:295–300.
2. Jones CU, Hunt D, McGowan DG, Amin MB, Chetner MP, Bruner DW, et al. Radiotherapy and short-term androgen deprivation for localized prostate cancer. N Engl J Med 2011;365:107–18.

3. Zelefsky MJ, Reuter VE, Fuks Z, Scardino P, Shippy A. Influence of local tumor control on distant metastases and cancer related mortality after external beam radiotherapy for prostate cancer. J Urol 2008;179:1368–73.
4. Wo JY, Zietman AL. Why does androgen deprivation enhance the results of radiation therapy? Urol Oncol 2008;26:522–9.
5. Jain RK, Safabakhsh N, Sckell A, Chen Y, Jiang P, Benjamin L, et al. Endothelial cell death, angiogenesis, and microvascular function after castration in an androgen-dependent tumor: role of vascular endothelial growth factor. Proc Natl Acad Sci U S A 1998;95:10820–5.
6. Al-Ubaidi FL, Schultz N, Egevad L, Granfors T, Loseva O, Helleday T. Castration therapy results in decreased Ku70 levels in prostate cancer. Clin Cancer Res 2013;19:1547–56.
7. Pollack A, Salem N, Ashoori F, Hachem P, Sangha M, von Eschenbach AC, et al. Lack of prostate cancer radiosensitization by androgen deprivation. Int J Radiat Oncol Biol Phys 2001;51:1002–7.
8. Lin C, Yang L, Tanasa B, Hutt K, Ju BG, Ohgi K, et al. Nuclear receptor-induced chromosomal proximity and DNA breaks underlie specific translocations in cancer. Cell 2009;139:1069–83.
9. Schiewer MJ, Goodwin JF, Han S, Brenner JC, Augello MA, Dean JL, et al. Dual roles of PARP-1 promote cancer growth and progression. Cancer Discov 2012;2:1134–49.
10. Scher HI, Fizazi K, Saad F, Taplin ME, Sternberg CN, Miller K, et al. Increased survival with enzalutamide in prostate cancer after chemotherapy. N Engl J Med 2012;367:1187–97.
11. de Bono JS, Logothetis CJ, Molina A, Fizazi K, North S, Chu L, et al. Abiraterone and increased survival in metastatic prostate cancer. N Engl J Med 2011;364:1995–2005.
12. Tran C, Ouk S, Clegg NJ, Chen Y, Watson PA, Arora V, et al. Development of a second-generation antiandrogen for treatment of advanced prostate cancer. Science 2009;324:787–90.
13. Clegg NJ, Wongvipat J, Joseph JD, Tran C, Ouk S, Dilhas A, et al. ARN-509: a novel antiandrogen for prostate cancer treatment. Cancer Res 2012;72:1494–503.
14. Taylor BS, Schultz N, Hieronymus H, Gopalan A, Xiao Y, Carver BS, et al. Integrative genomic profiling of human prostate cancer. Cancer Cell 2010;18:11–22.
15. Hieronymus H, Lamb J, Ross KN, Peng XP, Clement C, Rodina A, et al. Gene expression signature-based chemical genomic prediction identifies a novel class of HSP90 pathway modulators. Cancer Cell 2006;10:321–30.
16. Carver BS, Chapinski C, Wongvipat J, Hieronymus H, Chen Y, Chandarlapaty S, et al. Reciprocal feedback regulation of PI3K and androgen receptor signaling in PTEN-deficient prostate cancer. Cancer Cell 2011;19:575–86.
17. Nelson PS, Clegg N, Arnold H, Ferguson C, Bonham M, White J, et al. The program of androgen-responsive genes in neoplastic prostate epithelium. Proc Natl Acad Sci U S A 2002;99:11890–5.
18. Gauss GH, Lieber MR. Unequal signal and coding joint formation in human V(D)J recombination. Mol Cell Biol 1993;13:3900–6.
19. Gauss GH, Lieber MR. Mechanistic constraints on diversity in human V(D)J recombination. Mol Cell Biol 1996;16:258–69.
20. Pierce AJ, Johnson RD, Thompson LH, Jasin M. XRCC3 promotes homology-directed repair of DNA damage in mammalian cells. Genes Dev 1999;13:2633–8.
21. Stark JM, Pierce AJ, Oh J, Pastink A, Jasin M. Genetic steps of mammalian homologous repair with distinct mutagenic consequences. Mol Cell Biol 2004;24:9305–16.
22. Sharma NL, Massie CE, Ramos-Montoya A, Zecchini V, Scott HE, Lamb AD, et al. The androgen receptor induces a distinct transcriptional program in castration-resistant prostate cancer in man. Cancer Cell 2013;23:35–47.
23. Grasso CS, Wu YM, Robinson DR, Cao X, Dhanasekaran SM, Khan AP, et al. The mutational landscape of lethal castration-resistant prostate cancer. Nature 2012;487:239–43.
24. Subramanian A, Tamayo P, Mootha VK, Mukherjee S, Ebert BL, Gillette MA, et al. Gene set enrichment analysis: a knowledge-based approach for interpreting genome-wide expression profiles. Proc Natl Acad Sci U S A 2005;102:15545–50.
25. Wang K, Singh D, Zeng Z, Coleman SJ, Huang Y, Savich GL, et al. MapSplice: accurate mapping of RNA-seq reads for splice junction discovery. Nucleic Acids Res 2010;38:e178.
26. Li B, Dewey CN. RSEM: accurate transcript quantification from RNA-Seq data with or without a reference genome. BMC Bioinformatics 2011;12:323.
27. Chen WT, Alpert A, Leiter C, Gong F, Jackson SP, Miller KM. Systematic identification of functional residues in mammalian histone H2AX. Mol Cell Biol 2013;33:111–26.